Materials & Design 222 (2022) 111082

Contents lists available at ScienceDirect

Materials & Design

journal homepage: www.elsevier.com/locate/matdes

Influence of geometrical notches and form optimization on the mechanical properties of additively manufactured lattice structures

Guillaume Meyer *, Haixu Wang, Christian Mittelstedt

Lightweight Construction and Design, Department of Mechanical Engineering, Technical University of Darmstadt, Darmstadt, Germany
Additive Manufacturing Center, Technical University of Darmstadt, Darmstadt, Germany

HIGHLIGHTS

- Notch reduction methods were applied to the truss bcc and f2ccz lattice structure unit cells.
- Promising numerical results leading to basic design rules were partially validated by experimental investigations.
- Challenges for the accurate manufacturing of such proposed shapes at small scale are identified.
- Based on observations, design guidelines are proposed.

GRAPHICAL ABSTRACT

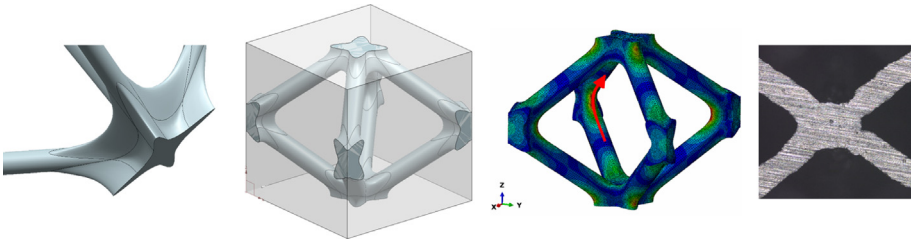

ARTICLE INFO

Article history:
Received 14 April 2022
Revised 4 August 2022
Accepted 19 August 2022
Available online 22 August 2022

Keywords:
Additive manufacturing
Lightweight design
Lattice structures
Notch effect
Stress reduction

ABSTRACT

Over the past decades, additive manufacturing technology has replaced the conventional methods of production of lattice structures such as investment casting, expanded metal sheet and metallic wire assembly. However, this technology still requires more development in order to enable the application of lattice structures in lightweight load bearing structures. The main challenge lies in the structural integrity of additively manufactured lattice structures which holds back exploiting their lightweight potential. While recent research focuses on the influence of process parameters on the mechanical behaviour of lattice structures, less attention is given to geometrical notches issued from sharp edges induced by the structural design. This contribution handles the effect of geometrically induced notches in truss lattice structures. The static mechanical properties of truss-like unit cells are compared to, on the one hand, the common design solution which consists in implementing a fillet radius and, on the other hand, two notch stress optimization methods inspired from existing methods for two-dimensional notches. The comparison encompasses the analytical development of the aforementioned methods as well as their numerical verification and experimental validation for additively manufactured lattices made of AlSi10Mg. Resulting recommendations on design guidelines for improved mechanical properties of truss lattice structures are then discussed.

1. Introduction

Porous and cellular structures of the most varied types and forms can be found almost everywhere in nature. Their lightweight potential has been recognized as one of the most promising engineering features to design load-bearing structures thanks to their advantageous specific mechanical properties [1,2]. With its recent

* Corresponding author at: Technische Universität Darmstadt, Fachbereich Maschinenbau, Fachgebiet Konstruktiver Leichtbau und Bauweisen, Otto-Berndt-Straße 2, 64287 Darmstadt, Germany.
E-mail address: guillaume.meyer@klub.tu-darmstadt.de (G. Meyer).

https://doi.org/10.1016/j.matdes.2022.111082
0264-1275/

development and expansion, additive manufacturing and the related promises towards the given design freedom enable mimicking nature's structures at different scales. At the meso-scale, and compared to porous structures, lattice structures offer the tailoring of mechanical property through their topology and are therefore predestined for the additive manufacturing technology [3].

Over the past years, research concentrates on the lightweight potential of lattice structures. Their mechanical behaviour towards compression loading has been identified as one the most promising features for lightweight industrial use [4]. Recent research focuses on the reliable manufacturing of lattice structures, as non-optimal process parameters lead to defects that have detrimental impact on the mechanical behaviour of lattice structures. Local texturing [5–7], porosity [8,9] and geometric deviations, such as strut diameter variation including surface roughness, strut waviness or offset of the lattice junction centre [10–13] can be listed among the defects creating notches responsible for local stress concentration. It is therefore of utmost importance to reduce their influence to improve the load-bearing capacity of lattice structures and exploit the lightweight potential of lattice structures to its greatest extent. However, difficulties can be encountered at the early stage of lattice design and modeling [16]. Nowadays, lattice structures are computed with the help of established commercial software or newer software specialized in the creation of parts for additive manufacturing with specific features for lattice structures. Open-source software with its own lattice library and coding are focus of current research [14,15]. Despite its apparent simplicity, the conception of lattice structures is time-consuming and prone to errors for detailed features such as the transition between unit cells. Specific mathematical approaches have been developed to tackle this issue, in particular regard of graded structures, but at the cost of generality [17,18]. One common solution to employ the developed formulations is the use of B-splines [19,20].

The junction centre of lattice struts, in the following denoted as nodal area, has been identified as the most critical area in terms of design induced notches by investigating the initial design via finite element analysis [21–24] and are even present after using lattice optimization routines [25–27]. Avoiding design notches is by definition a form optimization task, since general construction guidelines allowing complex shapes drawing near structures as observed in nature [28] are not available in the case of lattice structures. In order to avoid these notches in the truss lattice design, the literature offers mainly the single universal solution of a form or shape optimization by means of circular fillet radius [23,24,29–33] whereas other promising redesign tasks are meant to be load case specific [34,35]. According to the authors' best knowledge, a comparison between the influences of design notches and printing imperfection is not available as far as thin walled structures are concerned.

While the chosen circular fillet radius solution inarguably offers to deepen the lightweight potential of truss lattice structures, the available literature for notch optimization tends to show that it may not be the best universal solution for avoiding local peak stresses. In the case of flexural hinge shapes, Zelenika has demonstrated that the circular fillet shape is far less compliant than other alternative designs such as the prismatic and elliptical shapes or other historic approaches for stress concentration reduction in prismatic and wedge shaped elements such as the *Grodzinski shape*, a graphical approach of a parabolic shape [36], the *Baud shape*, a mathematical shape inspired from fluid dynamic [37], or the *Thum-Bautz shape*, an empirical shape developed for cases where the Baud fillet is not effective [38]. Zelenika has highlighted, among others, that the circular shape is subjected to 26 % more stresses than the Thum-Bautz shape [39]. In the case of a shaft shoulder under tensile loading, Mattheck, Scherrer and Sörensen have developed two methods: The *Pocket Calculator Method*, a shape based on mechanical considerations, and the *Tensile Triangle Method*, another graphical method aiming to reproduce similar results to the *Pocket Calculator Method*. These two methods were compared to other designs including the circular fillet shape and shape optimization results, successfully validated in experiment and confronted to shapes available in the nature such as trees or bones with bluffing similarities as results [40–43]. The obtained stress concentration reduction was verified by Castro in a similar analysis by considering a circular fillet shape, the *Grodzinski shape*, the *Baud shape* and the shape obtained from the *Tensile Triangle Method*, where the obtained stress concentration factors were lower than the circular fillet by 30 %, 38 % and 33 % respectively [44]. Similarly, Taylor has assessed the stress concentration factor for his *Load Curvature Method* and obtained theoretically better results than Mattheck, however without experimental validation [45]. These examples demonstrate the higher potential of other design solutions than the classical fillet radius, which, if correctly implemented into their structural design, could drastically improve the load-bearing behaviour of lattice structures.

The aim of the present paper is, on the one hand, to highlight the importance of geometrically induced notches in truss lattice structures by offering a first insight in the relevance of design notches when compared with manufacturing defects, and, on the other hand, in order to reduce their influence, to propose alternative use-case design solutions to the commonly used fillet radius. These alternative solutions are meant to avoid specific solutions derived from optimization or mathematical descriptions by proposing a simple and generic approach that could offer practitioners and researchers straightforward guidelines specific to lattice structures in order to rapidly design robust lightweight structures without requiring any specific background knowledge [41]. To do so, the static performance of the original configurations of two representative unit cells (RUCs) of truss lattice structures, being representative of both bending- and stretching-dominated behaviours of truss lattice structures, are compared numerically and experimentally to three notch reduction methods selected by the authors. While the first selected method considers the standard solution of a circular fillet radius that will be further called the *Fillet Radius Method* (FRM), the other selected methods are directly inspired from the aforementioned two-dimensional shape optimization verified approaches for notch reduction. These two methods were extended to the three-dimensional space for the application on the considered truss lattice structures. The *Pocket Calculator Method* (PCM) was selected based on mechanical consideration. The *Tensile Triangle Method* (TTM) offers itself as a natural contender since it is comparable to the PCM while being easier to develop and implement due to its graphical nature. Furthermore, both methods are comparable to shapes observable in the nature [42] and applicable to lattice structures. This contribution is divided into various parts. Design methodology and verification through finite element methods are the main part, since they shall lead to recommendation for potential design guidelines geared towards improved mechanical properties of truss lattice structures. The second part deals with the numerical investigation of the chosen design approaches in order to discuss the stress concentration factors [46] assessed for each configuration under static compression loading. In order to account for the supplementary mass involved by these design measures, the lightweight grade is introduced. The last part of this paper covers the experimental validation of additively manufactured AlSi10Mg lattices for one particular diameter as a proof of concept while identifying the challenges of accurately manufacturing such proposed shapes on a small scale. Finally, further design solutions to reduce notch stresses are discussed.

2. Material & methods

2.1. Lattice structure design

2.1.1. Selected unit cells

As this study focuses on the investigation of the applicability of alternative design solutions to geometrically induced notches in lattice structures and in order to limit the scope of the study, only two RUCs are investigated. The selected two RUCs in this work are the body-centred cubic (bcc, Fig. 1 a) and the double-face-centred with vertical struts (f2ccz, Fig. 1 b) cubic unit cells, which are representative of bending-dominated and stretching-dominated truss lattice structures respectively. According to published works about finite element analyses of additively manufactured cubic lattice structures using μCT data, the highest nodal stress concentration has been assessed for the bcc unit cell [10]. It is therefore expected that reducing these notch stresses would lead to the highest relative increase of the effective mechanical properties among truss lattices unit cells. The f2ccz unit cell has been selected because of its good performance in terms of stability, specific energy absorption and build time compared to other cubic truss lattice structures [47,48]. Thus, a further improvement on its mechanical properties by applying effective notch stress reduction methods is also of interest. In order to ensure the manufacturability of the two RUCs, the unit cells are modelled in a way that only nodes are present on the boundary of the specimen so that no half or quarter of struts need to be manufactured (Fig. 1).

2.1.2. Fillet radius method (FRM)

This method consists in implementing the well-established fillet radius onto the unit cell tangent to the strut edges in order to avoid notches. A schematic example of the FRM with a constant radius is provided in Fig. 2.

2.1.3. ***Pocket*** *Calculator* ***method (PCM)***

The PCM was developed in frame of the notch stress reduction in a stepped bar of diameter D_i subject to tensional loading. The principle of this method lies in the compensation of the lateral force F_Q, which is responsible for notch stresses, by the tangential force F_T issued from local nominal stress by optimizing the cross-sectional area of the shaft [40]. The principle is depicted in Fig. 3 (a). The angle α_i describes the angle between the first path of the multi-linearized PCM curve at its starting inflexion point. Each sharp angle determines an inflexion point. Depending on an empirically determined start angle α_1 and support angle $\alpha_0 = 0^\circ$, the tangential force F_T^i and the lateral force F_Q^i can be calculated. The rate of change of α and the subsequent amount of segments s can thus be assessed to achieve an optimal stress distribution. The two-dimensional shape of the PCM curve is determined using the Eq. (1) and Eq. (2), issued from [40].

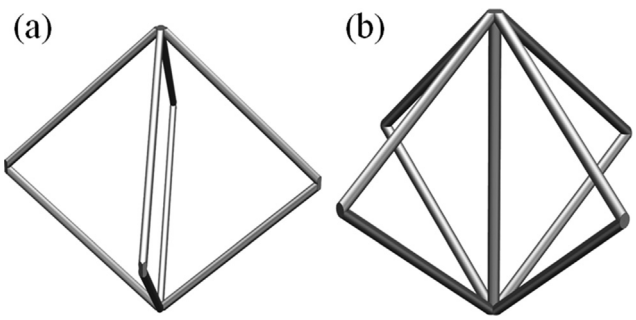

Fig. 1. Selected lattice structure unit cells – bcc (a) & f2ccz (b).

$$D_{i+1} = D_i + 2s\sin\left(\sum_{k=0}^{i}\alpha_k\right); \tag{1}$$

$$\alpha_{i+1} = 2 \times \arcsin\left(\frac{\frac{D_{i+1}}{D_i}\cos\left(\sum_{k=0}^{i-1}\alpha_k\right)\left(1+2\sin\left(\frac{\alpha_i}{2}\right)\right) - \cos\left(\sum_{k=0}^{i}\alpha_k\right)}{2\cos\left(\sum_{k=0}^{i}\alpha_k\right)}\right). \tag{2}$$

2.1.4. Tensile Triangle ***method (TTM)***

This graphical method inspired from shapes observed in nature such as tree or bones was developed to reduce the computational time of computer aided shape optimization and leads to shapes comparable to the PCM [42]. The sharp corner of a part is successively bridged with isosceles triangles (see Fig. 3 (b)) until a smooth transition is achieved. The optimal trade-off between mass increase and stress reduction is achieved for three triangles [43].

2.1.5. Application to lattice structure design

All CAD models were computed with the CAD software Siemens NX 11. The lattice unit cells were constructed manually and the relevant geometrical features that are cell size a, strut diameter d and curvature radius r_i (Fig. 7) were parametrized in order to facilitate generating any required configuration. It has to be noted that, although existing functionalities in CAD programs allow the direct implementation of the FRM on lattice structures using the built-in "fillet" function, a manual construction that bypasses the size limitation of the fillet radius, which is due to the complex geometry at nodal areas, was implemented for this method too.

The 2D curves of each aforementioned notch stress reduction methods are applied onto the nodal area of the unit cell. Depending on the unit cell configuration, the angle φ between each neighbouring strut varies. For the bcc unit cell, curves are constructed for the 109° and 70.53° angles while the f2ccz unit cell needs curves for the 45°, 60°, 90° and 120° angles as depicted in Fig. 4.

In order to be able to apply both PCM and TTM to the investigated unit cells, the bisection method as introduced by Mattheck is used [42]. This method, initially developed for the TTM, consists in halving the considered φ angle and applying twice the notch stress reduction method starting from the angle bisector. The bisection method is applied for the PCM curve too by considering a maximum angle $\alpha_{max} = 90^\circ - \varphi/2$, so that no inflection point is present at the intersection point of the PCM curve and the angle bisector. The PCM segment creation of both bcc and f2ccz cells is initiated at one of the curve's edges with a starting angle $\alpha_1 = 3^\circ$, an angle identified due to its wide applicability [40]. Both TTM and PCM curves are then smoothed using cubic spline. A construction example for $\varphi = 70.53^\circ$ is shown in Fig. 5 for all considered methods, with construction lines represented as dashed curves and the points A and B being the starting and ending points of the curves generated by PCM and TTM, respectively.

The transformation from the 2D curves into 3D is realized by constructing continuous surfaces using the curves and the unit cells themselves as boundary conditions. The surfaces are then sewn together with the struts to form a single solid RUC (Fig. 6).

For clarity purposes, all the described methods will be further assigned a constant curvature radius. In the case of PCM/TTM, the equivalent curvature radius corresponds to a constant radius at the angle bisector deployed by the FRM. This enables a comparison between the selected notch reduction methods. The bcc unit cell is described by one curvature radius r_1, whereas the f2ccz configuration is described by two curvature radii r_1 and r_2. The equivalent curvature radii have been parameterized depending on the

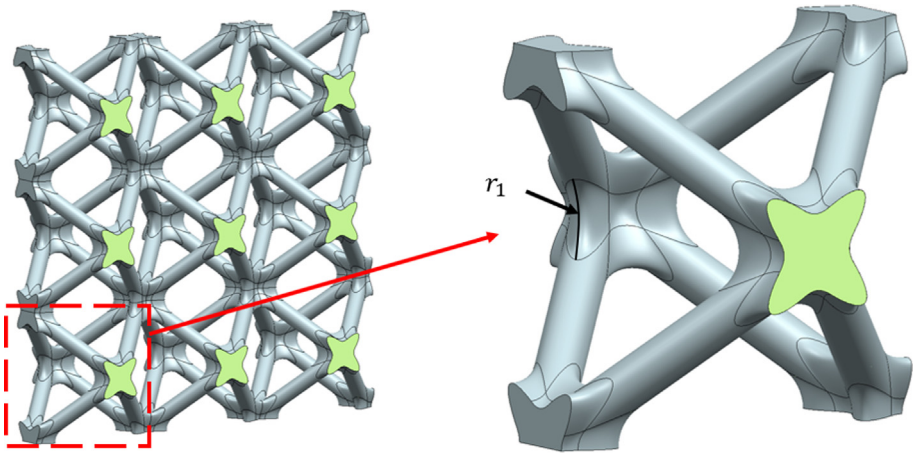

Fig. 2. Example of the Fillet Radius Method (FRM) in lattice structures.

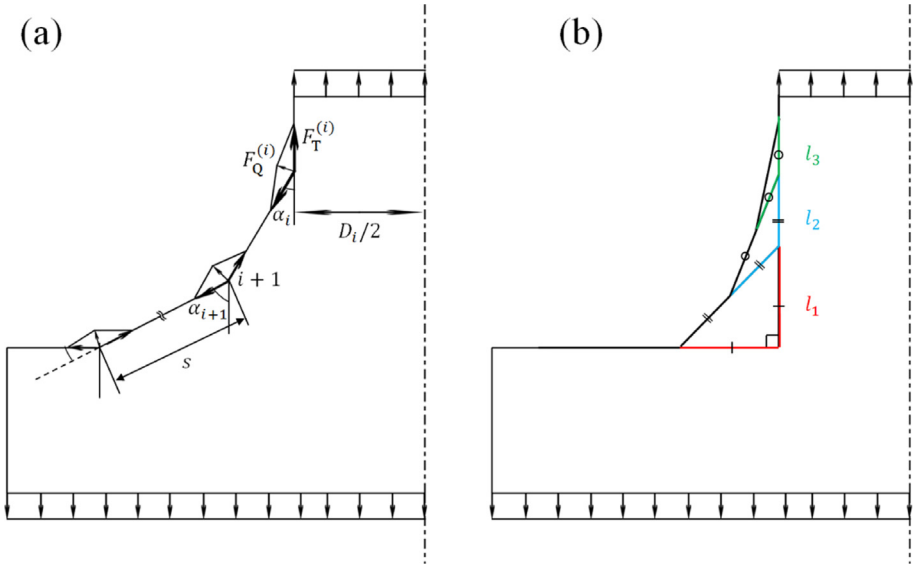

Fig. 3. Pocket Calculator Method (PCM) applied to a stepped bar with rotational symmetry under uniaxial tensile load (a) and Tensile Triangle Method (TTM) applied to a rectangular notch with 3 tensile triangles (b). Based on and recompiled from [40] and [42].

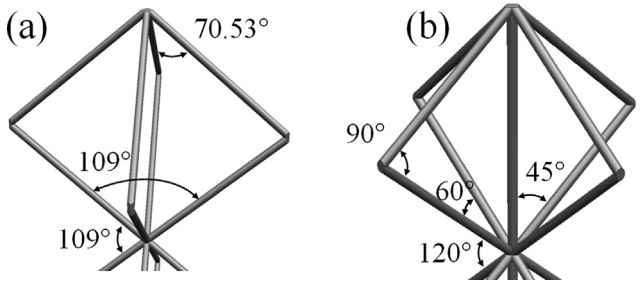

Fig. 4. Angle Selection for Curve Generation – bcc (a) & f2ccz (b).

modelled strut diameter d. To do so, the curvature factors γ and ϑ are introduced. Fig. 7 displays exemplarily both bcc and f2ccz unit cells for the PCM while both Eq. (3) and Eq. (4) show the curvature radius parametrization that will be further used in this paper.

$$r_1 = \gamma \cdot d \tag{3}$$

$$r_2 = \theta \cdot d \tag{4}$$

2.2. Numerical analysis

2.2.1. Finite element model

The numerical software ABAQUS was employed for the numerical investigation of the lattice structures. The finite element model consists of a single RUC under compression loading applied as homogeneous unitary displacement at its upper cross section while its lower cross section has been clamped as depicted in Fig. 8 and Fig. 9 in the respective cases of bcc and f2ccz. The modelled lattice structures were meshed using solid tetrahedron elements with 10-nodes and quadratic interpolation with local and global seed sizes respectively assigned to the nodal area and the lattice struts. The local seed size of both modelled unit cells yields 0.02 mm while the global seed size of the bcc unit cell (0.05 mm) differs from the one of the f2ccz unit cell (0.03 mm). The material properties used in this model are based on the values of the additively printed AlSi10Mg solid material that can be found in the literature: density $\rho_S = 2.67\text{g/cm}^3$ [49], Young's modulus in vertical directions $E_S = 70\text{GPa}$ [49] and Poisson's ratio $\upsilon = 0.35$ [50].

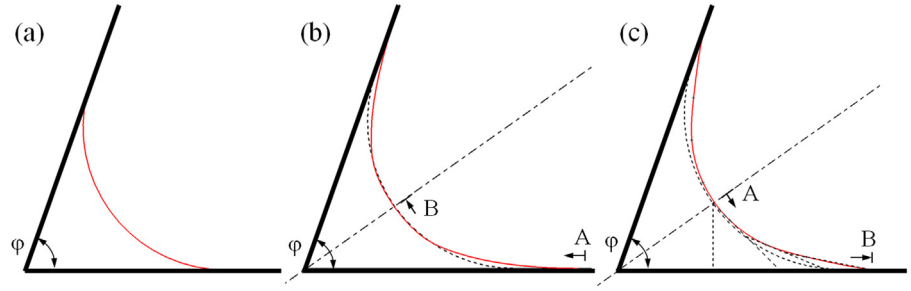

Fig. 5. Bisection of φ angle – Example for φ = 70.53° for FRM (a), PCM (b) & TTM (c).

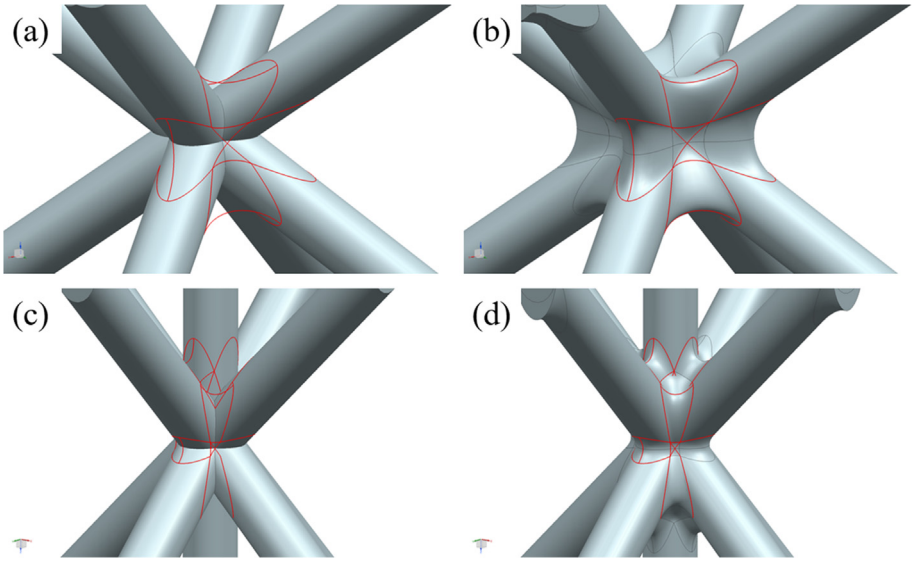

Fig. 6. Nodal Area Construction for Notch Stress Optimization Methods – from splines of (a) bcc& (c) f2ccz to RUC volumes (b) of bcc & (d) f2ccz.

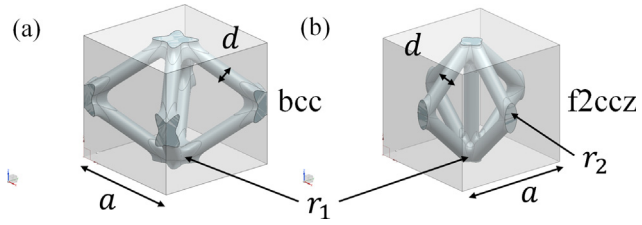

Fig. 7. CAD Models of the considered RUCs with exemplarily PCM applied – bcc (a) & f2ccz (b).

2.2.2. ***Notch*** *stresses assessment*

Notch stresses can be identified by means of stress concentration factors based on the stress distribution within the unit cell along a given path and can be expressed in the form given by Eq. (5), where σ_{max} is the peak stress and σ_{mean} the mean stress of an undisturbed area [46] while $x = 0$ and $x = \lambda$ correspond to both extremity of the stress path.

$$K_t = \frac{\sigma_{max}}{\sigma_{mean}} = \frac{max(\sigma(x))}{\sigma_{mean}}, x\epsilon[0, \lambda] \tag{5}$$

Although σ_{max} can be described by the maximum von-Mises stress experienced by the unit cell in both cases, the different stress distributions inherent to the different loading states lead to separate assessments of σ_{mean}. On the one hand, the bending-dominated bcc unit cell yields a homogeneous stress distribution within its struts under compression loading [10]. Hence, for bcc, σ_{mean} is considered as the minimum mean von-Mises stress of the unit cell and σ_{max} is assessed along a load path starting and ending at two strut halves respectively located at the upper and lower halves of the unit cell (Fig. 10 (a)). On the other hand, the stretching-dominated f2ccz cell sees its vertical strut, if aligned to the loading direction, carrying almost exclusively the complete load [10], leaving inclined struts not involved into the structural load bearing behaviour. Thus, σ_{mean} is extracted from the minimum mean von-Mises stress of the vertical strut and the considered load path starts from the strut half of an inclined strut and ends at the middle point of the vertical strut of the unit cell (Fig. 10 (b)).

In order to allow a quantitative comparison between the methods for similar equivalent curvature radius, the lightweight grade L^* (Eq. (6)) is introduced. It is the inverse of the specific stress concentration factor and the relative density $\bar{\rho}$ of the considered unit cell. Therefore, the optimal configuration describes an improvement of the mechanical properties that outgrows the disadvantage brought by the additional mass due to a given curvature.

$$L^* = \left(K_t \times \bar{\rho}\right)^{-1} \tag{6}$$

2.3. Experimental setup

2.3.1. Sample manufacturing

The specimens were manufactured on an EOS M290 laser powder bed fusion system. Based on the established process window for the reliable manufacturing of AlSi10Mg lattice structures below

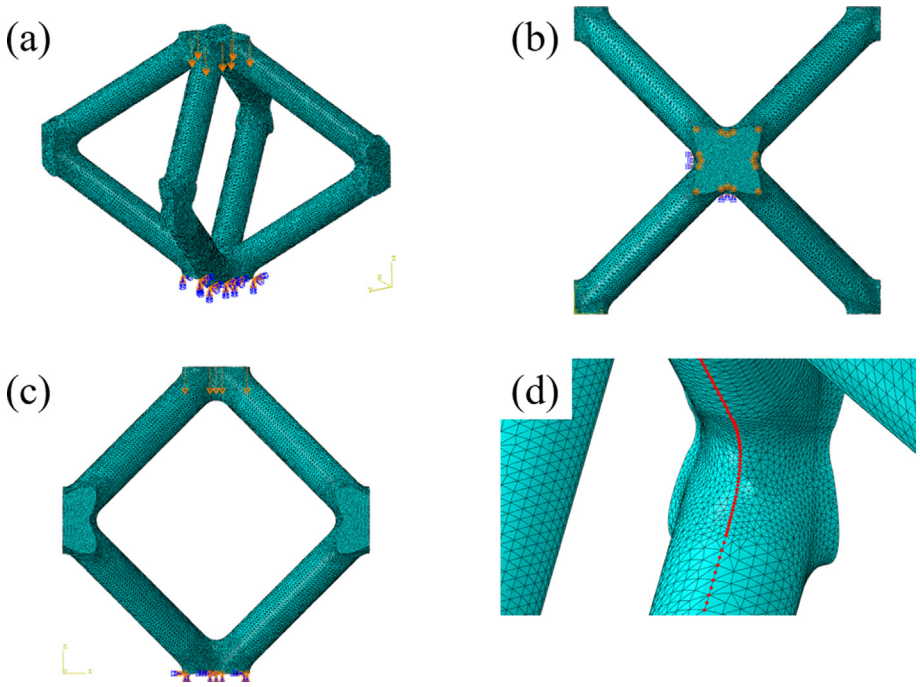

Fig. 8. Modelling example for the bcc cell (PCM): isometric view (a), top view (b), side view (c), nodal area (d).

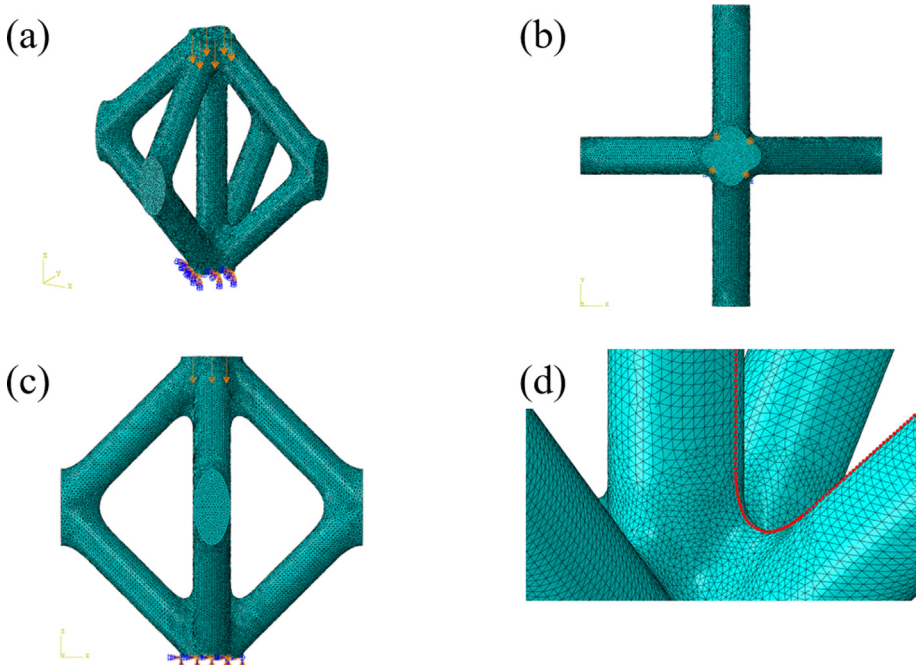

Fig. 9. Modelling example for the f2ccz cell (PCM): isometric view (a), top view (b), side view (c), nodal area (d).

400 µm published by Großmann that enables investigating high aspect ratios for reasonable sample size [9], a constant parameter set was selected in order to prevent from a potential influence of the manufacturing parameters on the mechanical properties of the investigated specimen. The sample geometry is made of 10x10x10 unit cells based on a 3 mm cell size *a* (Fig. 7), while the strut diameter *d* depends on process parameters and had to be measured after specimen manufacturing. All the relevant data are listed in Table 1.

2.3.2. Microscopic analysis

Before conducting compressive strength tests, the specimens were analysed microscopically with a ZEISS Axioskop A1 HAL 100 microscope with 50 × magnification. Contrary to [9], the strut diameters were directly measured on the specimen to be tested. To do so, each strut of a selected unit cell within the sample was measured separately (Fig. 11 (a)) and the strut thickness was obtained after averaging all the measurements. Furthermore, one supplementary sample of each specimen was ground in order to observe

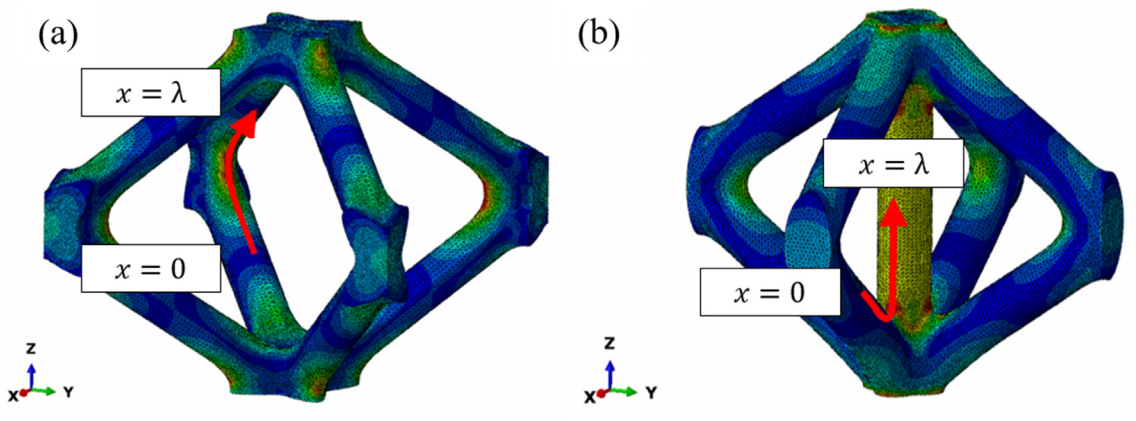

Fig. 10. Load Path for Stress Concentration Factor Assessment – bcc (a) & f2ccz (b).

Table 1
Sample manufacturing data.

Process parameter	Value	Unit
Cell size a	3	mm
Unit cells per direction	10x10x10	–
Base CAD diameter d	100	µm
Scanning strategy	Contour exposure	–
Laser power P	250	W
Laser scan speed v_S	2500	mm/s
Laser beam diameter d_L	80	µm
Layer thickness l_S	30	µm
Build platform temperature	125	°C

the nodal area (Fig. 11 (b)). Pictures of the cross section at half strut depth were obtained by grinding the lattice directly; i.e. without epoxy resin embedment; by means of tools especially manufactured for this purpose (Fig. 11 (c)).

2.3.3. ***Density*** *measurement*

Archimedean density measurements were carried out based on the on the German engineering norm DIN 3369:2010 [51] with an assumed solid density $\rho_S = 2.67 g/cm^3$ [49] in order to identify potential increased porosity in the nodal area and, therefore, to establish a relationship between the fillet curvature and the material density of the manufactured specimens.

2.3.4. Compression ***tests***

Uniaxial static compression tests were conducted in accordance with the German engineering norm DIN EN 50134:2008-10 [52] using a Zwick/Roell Z100 testing machine. Through the experiment, the effective Young's modulus E^* and the specific energy absorption $E_V^{'}$ until compressive failure of each specimen were assessed in order to establish a potential influence of the notch reduction methods on the relationship between the strength and the ductility of the investigated lattice structures. It is important to note that, similarly to Großmann and Weidmann [9,53], the determination of the plateau stress deviated from the standard. This consideration is due to the brittleness of the AlSi10Mg alloy, which yields a stochastic mechanical behaviour after reaching the compressive failure strain. Therefore, on the one hand, the calculation of the plateau stress R_{plt}, which was assessed through a preliminary test, was based on the first maximum compressive strength R_{eH} corresponding to the first local maximum in the stress–strain curve, as shown in Eq. (7) and, on the other hand, the specific energy absorption is calculated until the compressive failure strain.

$$R_{plt} = \frac{1}{2} R_{eH} \tag{7}$$

For the preliminary test, a constant strain rate of 2×10^{-3} s^{-1} was used. During the main compression test, a constant strain rate of 10^{-3} s^{-1} was used until the first maximum compressive strength and, after the first specimen failure, a constant strain rate of 10^{-2} s^{-1} was used until 40 % of the total strain was reached. The stiffness of the machine was considered by correcting the measured displacement of the crosshead.

3. Results

In the framework of this investigation, the focus has been purposely set on elastic properties in order to obtain a material independent influence of the introduced methods on the load path distribution within the chosen lattice unit cells. To do so, relative deviations of stress concentrations observed during FE simulations and the relative Young's modulus calculated from experiments have been considered. Deviations between numerical investigation and experiment are discussed accounting for manufacturing quality. Information gained from the plastic range were reported too

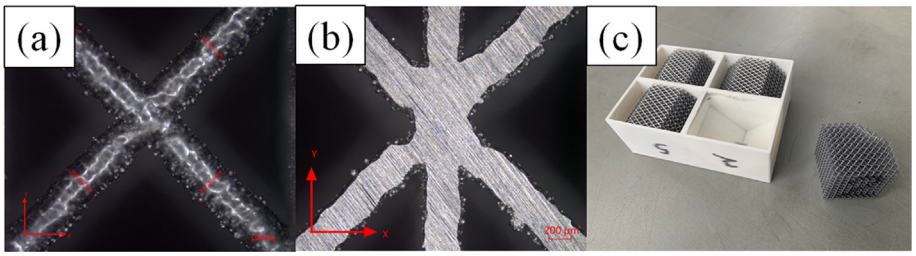

Fig. 11. Microscopic Analysis – strut measurement example (a), grinded sample example (b) & grinding tools (c).

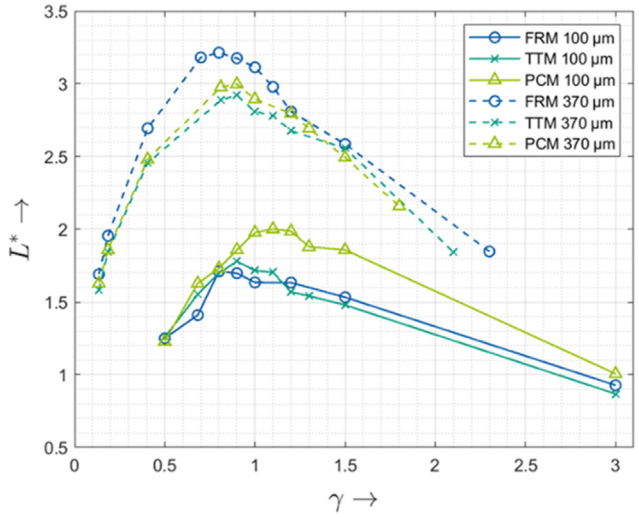

Fig. 12. Numerical results – bcc – Lightweight grade as function of the curvature radius.

Table 2
Numerical results – bcc – optimal configuration (R_2).

d [µm]	FRM		PCM		TTM	
	γ	L^*	γ	L^*	γ	L^*
100	0.8	1.71	1.1	2.00	0.9	1.78
370	0.8	3.22	0.9	3.00	0.9	2.92

for completeness and can be considered as additional data which could be useful for other researchers.

3.1. Numerical results

3.1.1. bcc

Fig. 12 shows the results obtained for the numerical analysis of bcc cells of 100 µm and 370 µm diameter. It can be noticed that for the 100 µm diameter cells, the optimal lightweight grade was obtained for PCM and outperforms FRM and TTM by 17 % and 12 % respectively, whereas FRM outperforms PCM and TTM by 7 % and 10 % respectively at 370 µm. The corresponding curvature radii and corresponding lightweight grades are reported in Table 2.

Fig. 13 displays the stress concentration variation for the selected notch reduction approaches exemplarily for $d = 375\mu$m. Different values of the maximum stress concentration factor K_t are plotted along the selected load path (Fig. 10). The initial configuration is compared to, on the one hand, a minimal equivalent curvature radius R_1 ($\gamma = 0.135$) and, on the other hand, the optimal equivalent curvature radius identified in Table 2 above. It can be noticed that the peak stress occurs for $x/\lambda = 0.5$, which can be expected since the nodal area is located in the middle of the normalized selected path. A decrease of the peak stress is already observed for the small curvature radius R_1, while R_2 offers a more drastic stress reduction with a smooth load redistribution (Fig. 14).

3.1.2. f2ccz

In the case of the f2ccz unit cell, two radii have to be varied (Fig. 7). During the numerical investigation, it has been noticed that the stress concentration is redistributed to diagonal struts for low values of θ. Fig. 15 demonstrates that the stress peak at the junction of diagonal struts increases drastically as γ gets larger, leading to a plateau of K_t at $\gamma = 0.3$ or above. Fig. 16 illustrates this load redistribution with examples for $\theta = 0.135$ and $\theta = 0.5$. The origin of the plateau lies in the fact that the selected load path does not cover the junction between diagonal struts (Fig. 10).

To prevent the effect of stress redistribution, $\theta = 0.5$ is kept constant for further investigations. This value may not lead to an optimal stress concentration at the junction of diagonal struts but it offers a sufficient load reduction so that the nominal stress is hardly affected by different values of θ. The maximum difference in nominal stress among the different models at $\gamma = 0.5$ is 0.6 %. Thus, it can be ensured that the stress concentration always occurs at junctions involving vertical struts.

Fig. 17 shows the results obtained for the numerical analysis of bcc cells of 100 µm and 370 µm diameter. It can be noticed that PCM outperforms FRM and TTM for both strut diameters, reducing specific notch stresses by about 16 % for both approaches at 100 µm, and being better by 20 % and 10 %, respectively, at 370 µm. The corresponding curvature radii and corresponding lightweight grades are reported in Table 3.

Fig. 18 displays the stress concentration variation for the selected notch reduction approaches exemplarily for $d = 375\mu$m.

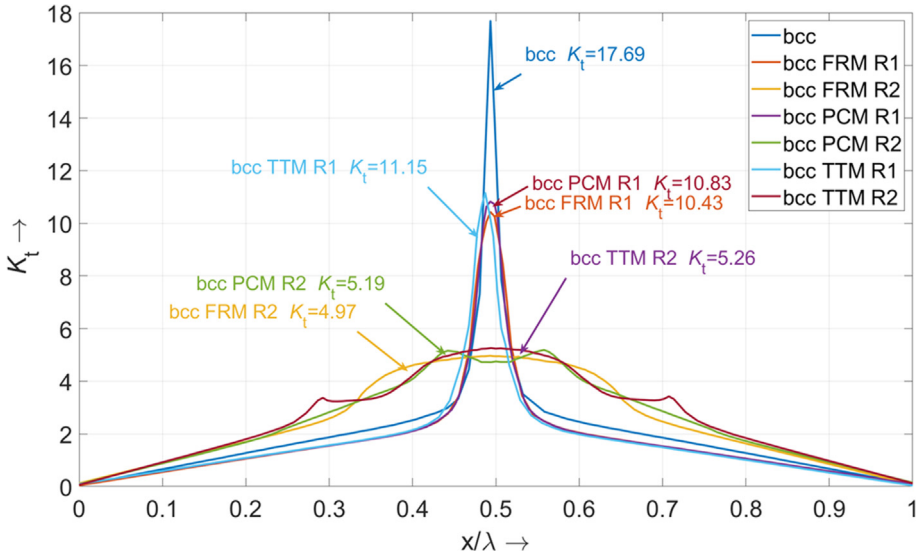

Fig. 13. Numerical results – bcc – Stress concentration distribution.

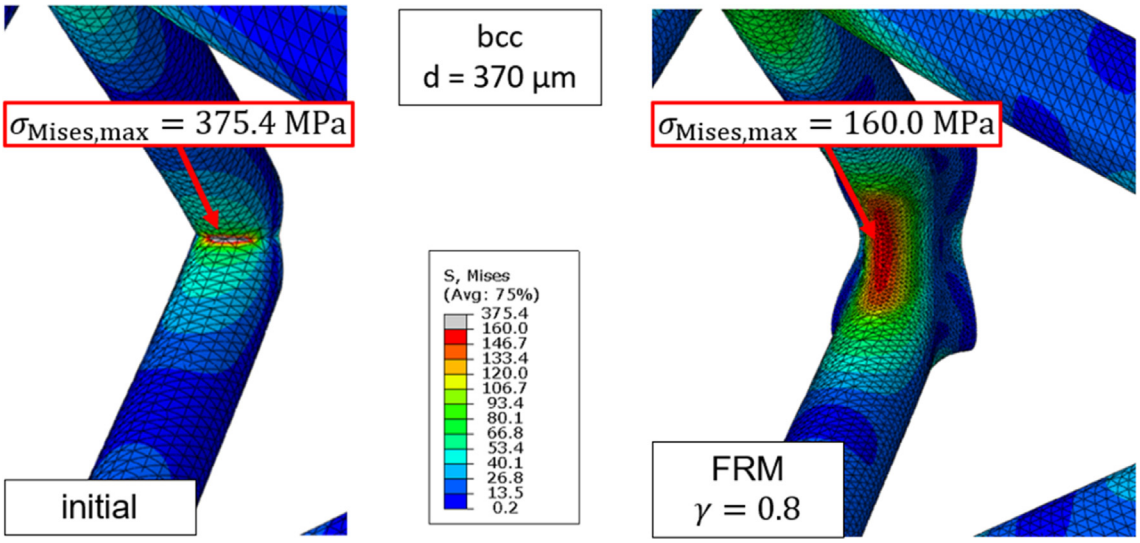

Fig. 14. Numerical results – bcc – Stress plots for initial (left) and optimal configuration (right).

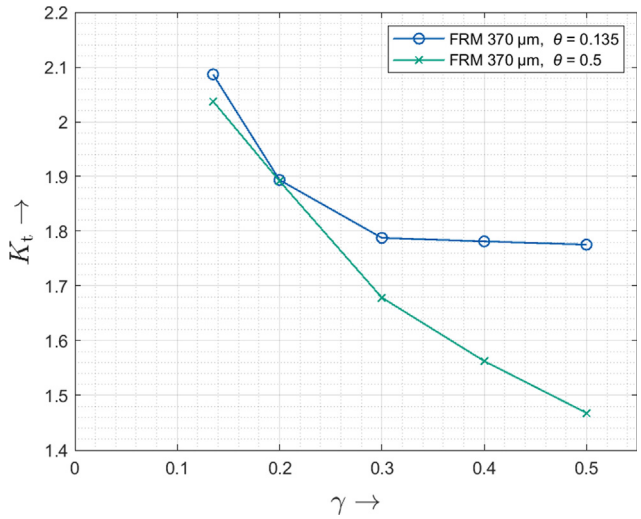

Fig. 15. Numerical results – f2ccz – Stress concentration variation.

The maximum stress concentration factor K_t for optimal configuration is shown in Table 3 above . Contrary to the bcc unit cell, only the optimal equivalent curvature radius is plotted for better readability. The initial f2ccz peak stress is located at $x/\lambda = \frac{1}{2} \cdot \arccos\left(45^{\circ}\right)$ due to the selected load path (Fig. 10). It can be noticed that the stress concentration is not only reduced but the peak stress is redistributed into two separate smaller peak stresses (Fig. 19).

3.2. Experimental ***results***

In the frame of the experimental investigation, 5 samples of each considered configuration were investigated. As for the numerical part, the initial unit cell configurations are compared to, on the one hand, a minimum equivalent curvature radius R_1 ($\gamma = 0.135$) and, on the other hand, the identified optimal equivalent curvature radius R_2 (Table 2, Table 3). The value $\theta = 0.5$ is considered for the investigation of f2ccz unit cell as well. Due to manufacturing constraints, only strut diameters of 370 µm were investigated. During a preliminary investigation, the employed manufacturing parameters described in Table 1 lead to an average as-built strut diameter

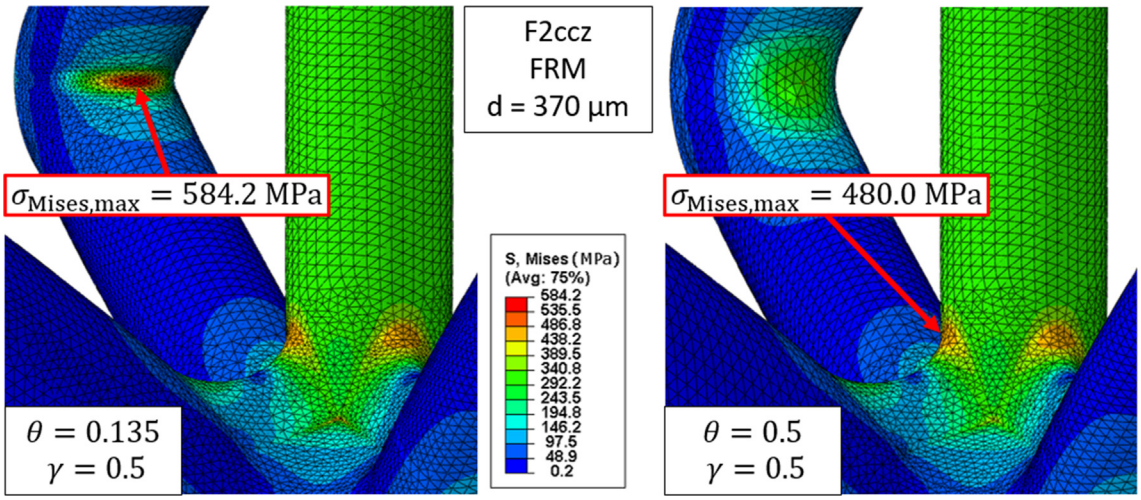

Fig. 16. Numerical results – f2ccz – Stress redistribution for θ variation.

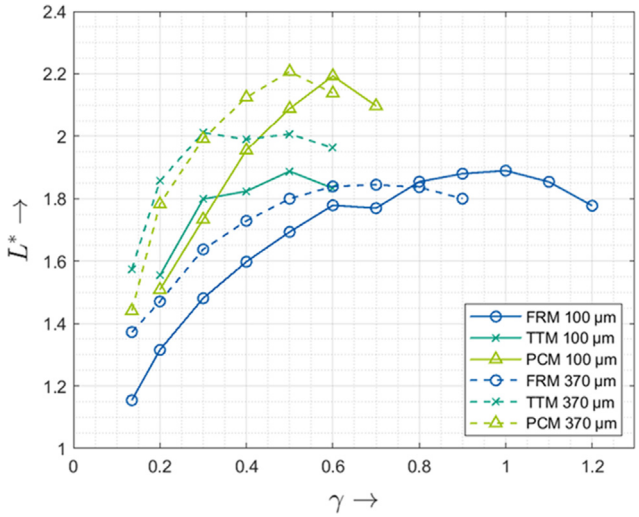

Fig. 17. Numerical results – f2ccz – Lightweight grade as function of the curvature radius.

Table 3
Numerical results – f2ccz – optimal configuration (R_2).

d [µm]	FRM		PCM		TTM	
	γ	L^*	γ	L^*	γ	L^*
100	1.0	1.89	0.5	2.19	0.6	1.89
370	0.6	1.84	0.5	2.21	0.3	2.01

of $370 \pm 13 \mu m$ for 4 printed samples of the 14 investigated configurations.

3.2.1. bcc

Fig. 20 depicts the stress–strain curves while Fig. 21 and Fig. 22 show the results obtained in the framework of the experimental investigation of the bcc unit cell. The brittle behaviour of as-built AlSi10Mg can be identified by the absence of a plateau stress and the consecutive stress peaks standing for sequential load redistribution and consecutive failure. An overall increase in effective Young's moduli estimated by means of hysteresis at R_2 compared to R_1 can be identified. Whereas R_1 do not show significant

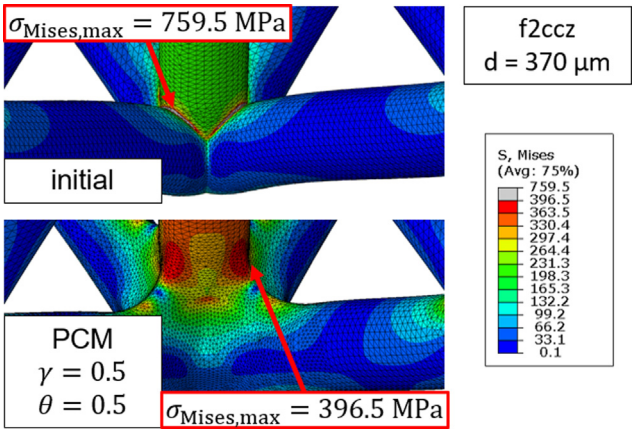

Fig. 19. Numerical results – f2ccz – Stress plots for initial (top) and optimal configuration (bottom).

improvement compared to the initial configuration. A similar trend is observed from both first maximum compressive strength and energy absorption per unit volume until compressive failure. However, the values for FRM at R_2 are slightly lower than what could be expected. As far as the linear elastic range is concerned, these observations demonstrate a good correlation with numerical results. A trend between the relative material density of the specimens and the size of the fillet curvature cannot be established.

3.2.2. f2ccz

Fig. 23 depicts the stress–strain curves while Fig. 24 and Fig. 25 show the results obtained in the framework of the experimental investigation of the f2ccz unit cell. Similar to the bcc structures, a brittle behaviour can be observed for f2ccz cells too. Unlike the numerical results for bcc, no significant trend for increasing equivalent curvature radius can be identified. Only slight improvements from the original configuration in terms of effective stiffness and energy absorption can be noticed. Compared to bcc specimens, the f2ccz samples have a lower relative material density.

3.2.3. Manufacturing quality

In order to provide more arguments for discussion, Fig. 26 and Fig. 27 offer an insight into the manufacturing quality of the bcc

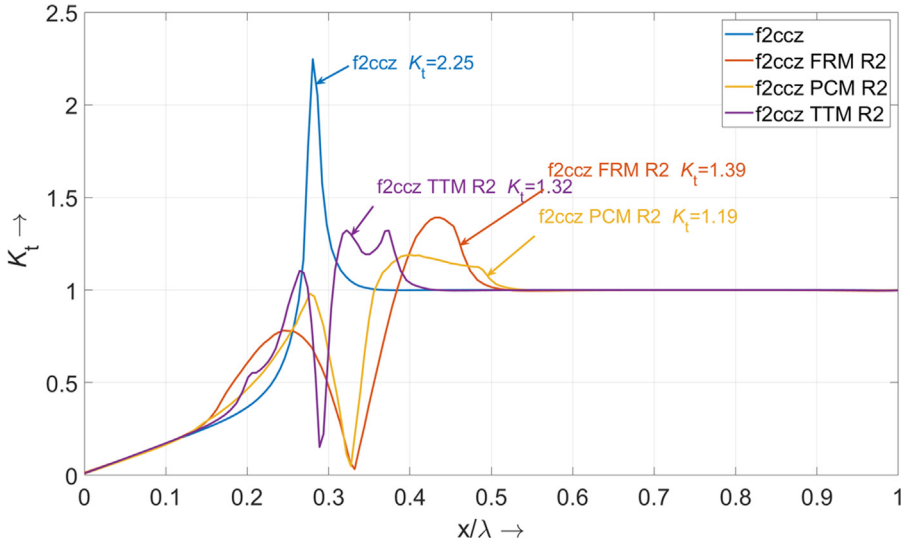

Fig. 18. Numerical results – f2ccz – Stress concentration distribution.

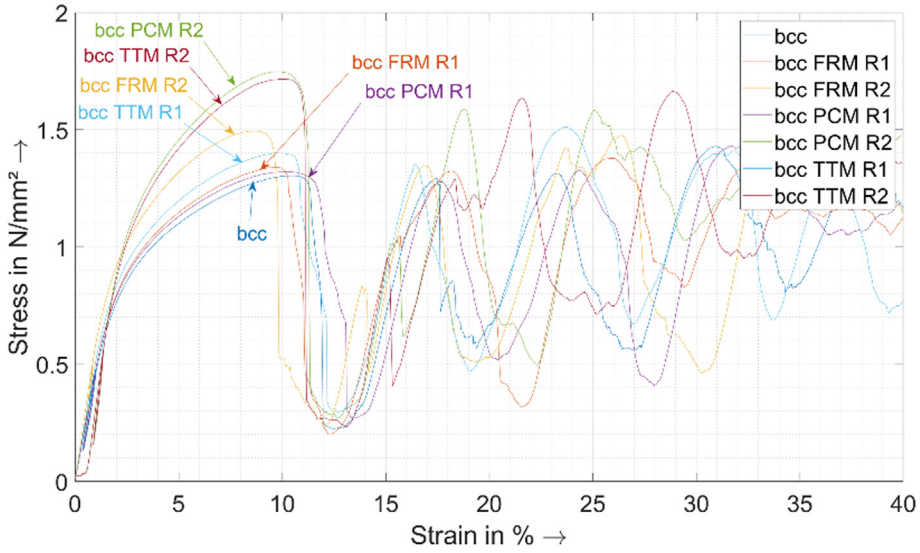

Fig. 20. Experimental results – bcc – stress strain curve.

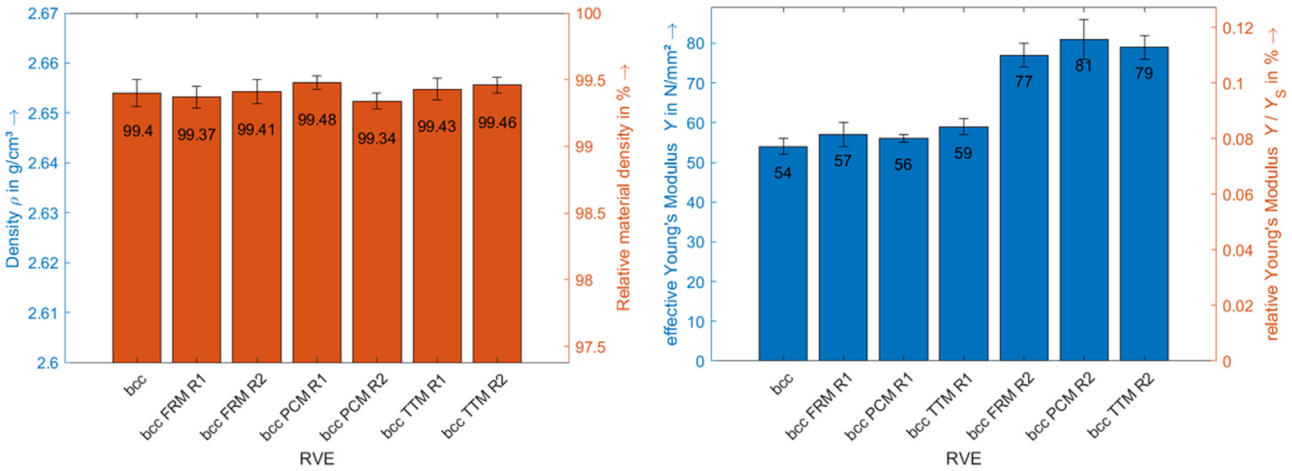

Fig. 21. Experimental results – bcc – density (left) & Young modulus (right).

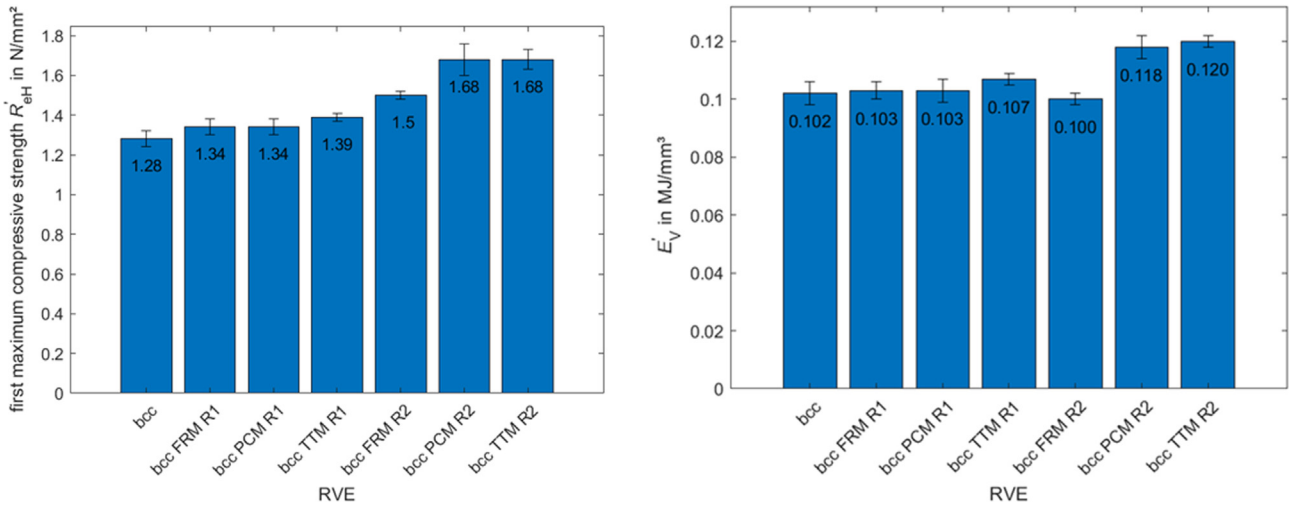

Fig. 22. Experimental results – bcc – first maximum compressive strength (left) & energy absorption (right).

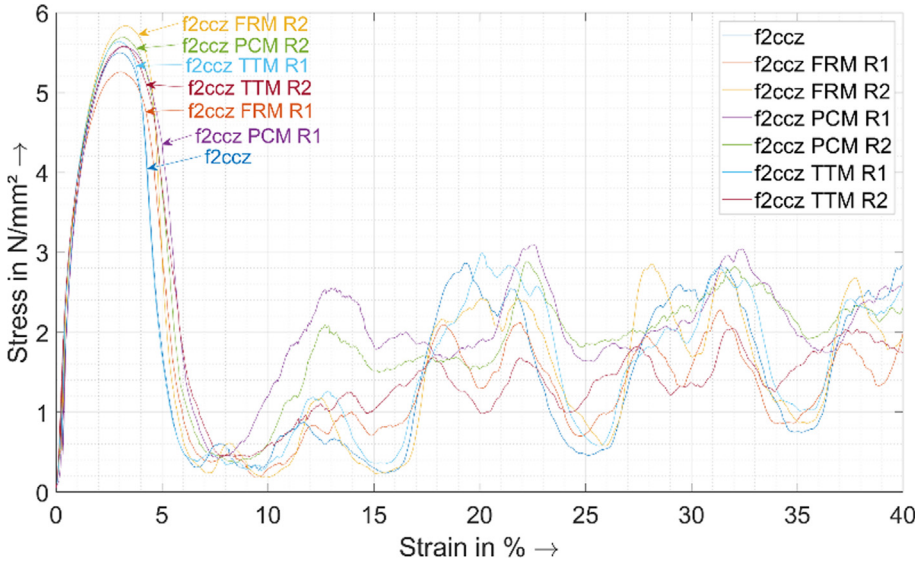

Fig. 23. Experimental results – f2ccz – stress strain curve.

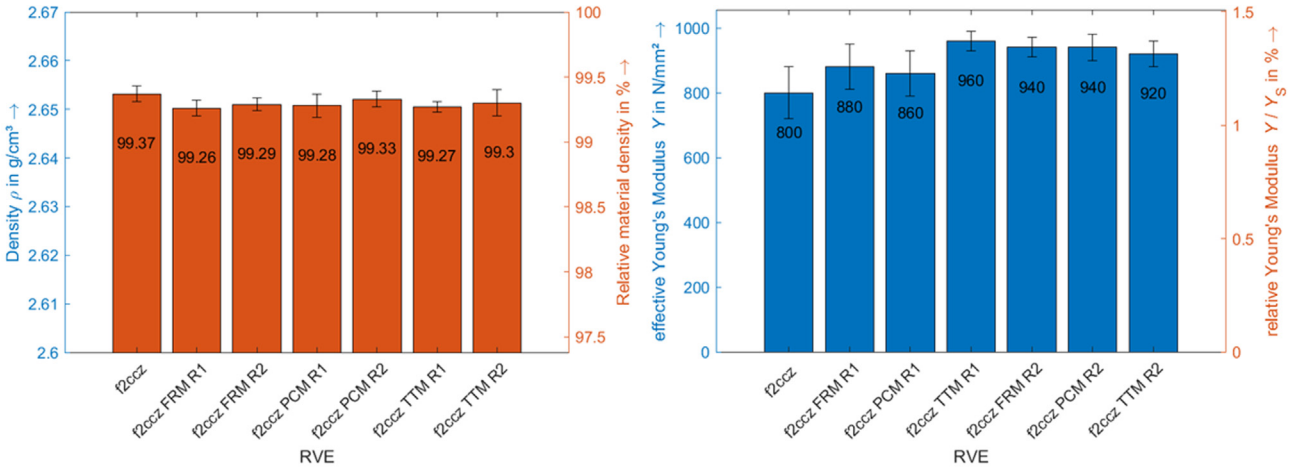

Fig. 24. Experimental results – f2ccz – density (left) & Young modulus (right).

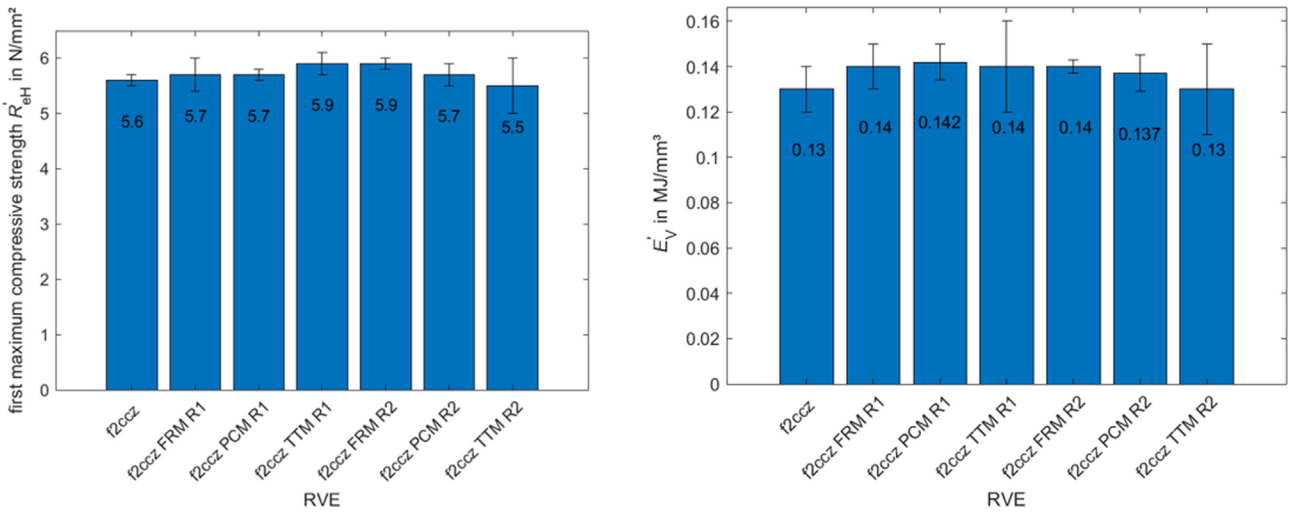

Fig. 25. Experimental results – f2ccz – first maximum compressive strength (left) & energy absorption (right).

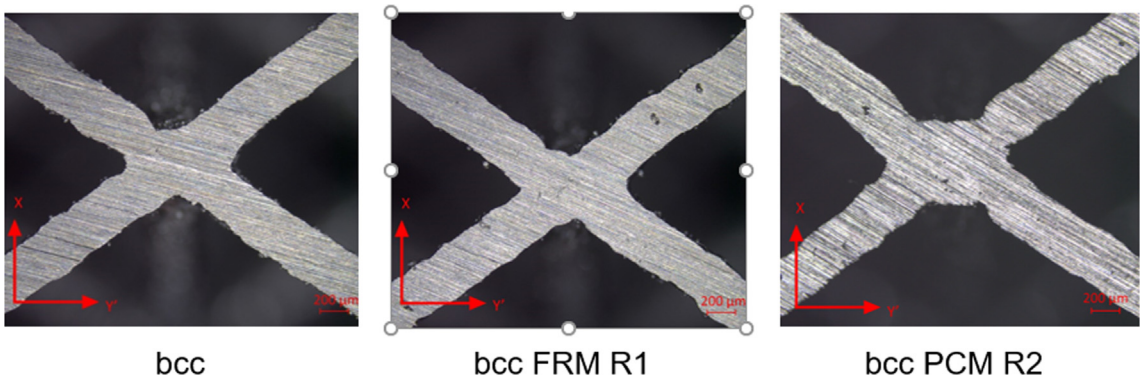

Fig. 26. Insight in manufacturing quality – bcc – initial configuration (left), FRM at R_1 (centre) and PCM at R_2 (right).

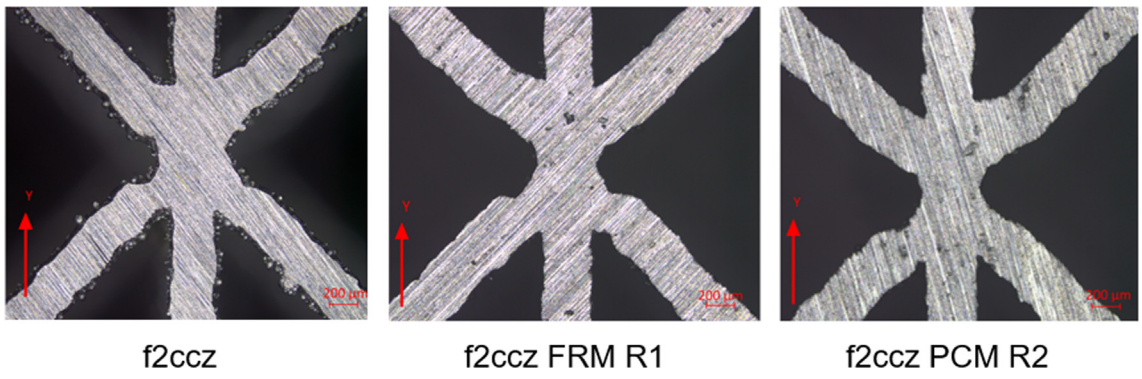

Fig. 27. Insight in manufacturing quality – f2ccz – initial configuration (left), FRM at R_1 (centre) and PCM at R_2 (right).

and f2ccz lattices, respectively. Overall, it can be observed that lateral fillets were better built than those at both up- and down-skin areas. A significant change in shape is only noticeable for bcc at R_2, with a visible increase in the fillet curvature size. Apart from an apparent slightly smoother transition at the up-skin area of R_2, clear differences between f2ccz unit cells are not distinguishable. Compared to the bcc samples, a lateral bottlenecking of the nodal area of f2ccz cells can be identified.

3.3. Discussion

The results demonstrate the potential of the selected notch reduction methods. As the stress is more homogenously distributed for increased sizes of fillet curvature, the ability of the specimen to resist deformation is increased too.

The theoretically better performance of PCM and TTM methods compared to FRM for f2ccz and bcc at small scale can be explained through the approach they follow. PCM and TTM were developed based on the notch stress appeared on a stepped bar [43]. TTM being a simplified graphical approach of PCM, it will always result in at most equivalent stress concentration reduction and therefore lead to at best similar mechanical gain in performance. This notch reduction method is particularly effective for lattice structures with extremely thin struts ($d = 100\mu$m) since they can be idealized as perfect truss structures with reduced nodal areas. Moreover, this method can be expected to be valid for f2ccz lattice structures with higher strut thickness since the vertical strut of the unit cell can be interpreted as a bar with a sharp edge which leads to the notch stress in the vicinity of the loading direction. FRM delivers better results for bcc structures at higher strut thickness due to, the more complex loading in the nodal area since the struts are not aligned with the load direction. Additionally, the better design combination of a constant curvature radius and the symmetry of the bcc unit cell offers a smoother and better load stress reduction. Therefore, for constant strut thickness within a given lattice structure, FRM is recommended for bcc unit cells and PCM is recommended for f2ccz structures. In the case of f2ccz, TTM could be a robust design alternative if the CAD implementation of PCM reveals itself to be complicated. Furthermore, it has to be mentioned that the fillet curvature shall not be indefinitely increased for the following two reasons: Firstly, the stress reduction shall be weighed (or "lightweighed") with the additional mass involved by a radius. Secondly, newly formed sharp edges may occur after load redistribution on the fillet perpendicular to the notches increase stress concentration (Fig. 19). These new stress concentrations could eventually outgrow intended notch stress reduction at the fillet and render the new design obsolete.

As far as the bcc specimens are concerned, the experimental results confirm the numerical trends. Despite potential manufacturing defects, the notch reduction concepts can be validated. The stress concentration occurs in the inner lateral part of the strut junction (Fig. 10 (a), Fig. 14), which is the most reliably manufactured nodal feature of the bcc structures. However, the manufacturing defects seem to have a significantly higher influence on the mechanical properties of the f2ccz structures, which is in line with the observations made by Leary [10]. However, similar to Dallago [54], applying notch reduction methods to f2ccz structures do help, just in a restricted manner. The reason for the limited impact of notch reduction methods is the lack of visible geometric difference. This is mostly due to the staircase effect [55] that hinders the differentiation of the already subtly different fillet shapes at the small scale. In the framework of this study, the relationship between the design space occupied by the implemented curvature radius (about 100 μm) is equivalent to some layers of printed

material only (Table 1). This results in difficulties for precise and accurate reproduction of the CAD geometries. The effect of different layer thicknesses on the dimensional accuracy of the fillet curvature shape is, however, not further investigated in the framework of this contribution. Another potential contributor to inaccuracies is the instable melt pool behaviour in the nodal area. This instability is due to, on the one hand, the high of number of struts joining together in this area (e.g. up to 10 for f2ccz) and, on the other hand, the contour strategy used for manufacturing [9]. This is in good agreement with the fact that bcc specimens have higher relative material density compared to the f2ccz ones since they have less struts joining at the nodal area. However, no noticeable influence of curvature radius on porosity was identified, which means that it does not have a direct influence on the melt pool for the selected manufacturing parameters.

Conclusively, it can be stated that the size of the fillet curvature plays a more significant role in determining the mechanical properties of the specimen compared to the influence of different notch optimization methods used at such small scale. The experimental result of bcc FRM at R_1 do not demonstrate the theoretical advantage over PCM or TTM which is explained by the geometric similarities due to manufacturing constraints. At larger scale, where the reliable manufacturability of fillet curvatures shall be ensured, the proposed design rules should follow the presented numerical results and considerably increase the mechanical properties as well [54].

4. Summary and conclusions

In the framework of this study, notch reduction methods were applied to bcc and f2ccz lattice structures that were additively manufactured with AlSi10Mg. The commonly used fillet radius was confronted to 2D notch stress optimization approaches that can be found in the literature. For this purpose, parametrized CAD-models were developed, and the 2D notch stress optimization methods are implemented into 3D lattice structures. Promising numerical results leading to basic design rules, that were partially validated by experimental investigations despite the influence of the staircase effect that prevents from faithfully retrieving the designed curvatures at small scale. In case of bcc structures, the FRM is recommended whereas the PCM or even the TTM are more advantageous for f2ccz lattice cells. It was demonstrated that, at small scale, the size of the equivalent curvature radius plays a preponderant role. Furthermore, it was proved that increasing the radius indefinitely may lead to potentially dangerous redistributed stress peaks. It is shown that the structural lightweight grade is of utmost importance for the increase of specific properties of lattice structures.

Future work will investigate on the applicability of these approaches to all further strut-based lattice structures of different cell sizes and diameters. So far, lattice structures with an overall constant strut thickness were investigated. In the framework of the implementation of lattice structures, these approaches will be considered for graded lattice structures as well. In case of promising results, a benchmark analysis considering other approaches found in literature is of highest relevance. Another relevant field of investigation is the application of the described approaches to other materials other than AlSi10Mg in as-built state. This would enable a deeper investigation of the influence of the proposed notch reduction methods in the plastic range. It could be of further interest to investigate the performance of such approaches for different load cases such as tension, shear or bending. Another potential field of area would be the systematic integration of these approaches into a CAD software. Modelling difficulties are expected by the author in the case of more complex structures. With the reliable implementation and manufacturing of notch reduction methods, improved mechanical properties of lattice structures such as fatigue or energy absorption may drastically increase the lightweight potential of these already promising cellular structures.

CRediT authorship contribution statement

Guillaume Meyer: Conceptualization, Methodology, Validation, Writing – original draft, Writing – review & editing, Visualization, Supervision. **Haixu Wang:** Software, Formal analysis, Investigation, Data curation, Writing – original draft, Writing – review & editing. **Christian Mittelstedt:** Writing – review & editing, Supervision, Project administration.

Declaration of Competing Interest

The authors declare that they have no known competing financial interests or personal relationships that could have appeared to influence the work reported in this paper.

Acknowledgement

We acknowledge support by the Open Access Publishing Fund of Technical University of Darmstadt.

References

[1] M.F. Ashby, R.F.M. Medalist, The mechanical properties of cellular solids, MTA 14 (9) (1983) 1755–1769, https://doi.org/10.1007/BF02645546.
[2] N.S. Ha, G. Lu, A review of recent research on bio-inspired structures and materials for energy absorption applications, Compos. B Eng. 181 (2020) 107496, https://doi.org/10.1016/j.compositesb.2019.107496.
[3] L.J. Gibson, M.F. Ashby, Cellular Solids: Structure and Properties, Cambridge University Press, 1997.
[4] T. Maconachie, M. Leary, B. Lozanovski, X. Zhang, M.a. Qian, O. Faruque, M. Brandt, SLM lattice structures: Properties, performance, applications and challenges, Mater. Des. 183 (2019) 108137, https://doi.org/10.1016/j.matdes.2019.108137.
[5] T. Niendorf, F. Brenne, M. Schaper, Lattice structures manufactured by SLM: on the effect of geometrical dimensions on microstructure evolution during processing, Metall. Mater. Trans. B 45 (4) (2014) 1181–1185, https://doi.org/10.1007/s11663-014-0086-z.
[6] X. Wang, J.A. Muñiz-Lerma, O. Sánchez-Mata, M. Attarian Shandiz, M. Brochu, Microstructure and mechanical properties of stainless steel 316L vertical struts manufactured by laser powder bed fusion process, Mater. Sci. Eng., A 736 (2018) 27–40, https://doi.org/10.1016/j.msea.2018.08.069.
[7] G. Meyer, F. Brenne, T. Niendorf, C. Mittelstedt, Influence of the miniaturisation effect on the effective stiffness of lattice structures in additive manufacturing, Metals 10 (11) (2020) 1442, https://doi.org/10.3390/met10111442.
[8] S.L. Sing, F.E. Wiria, W.Y. Yeong, Selective laser melting of lattice structures: A statistical approach to manufacturability and mechanical behavior, Rob. Comput. Integr. Manuf. 49 (2018) 170–180, https://doi.org/10.1016/j.rcim.2017.06.006.
[9] A. Großmann, J. Gosmann, C. Mittelstedt, Lightweight lattice structures in selective laser melting: design, fabrication and mechanical properties, Mater. Sci. Eng., A 766 (2019) 138356, https://doi.org/10.1016/j.msea.2019.138356.
[10] M. Leary, M. Mazur, J. Elambasseril, M. McMillan, T. Chirent, Y. Sun, M.a. Qian, M. Easton, M. Brandt, Selective laser melting (SLM) of AlSi12Mg lattice structures, Mater. Des. 98 (2016) 344–357, https://doi.org/10.1016/j.matdes.2016.02.127.
[11] M. Mazur, M. Leary, S. Sun, M. Vcelka, D. Shidid, M. Brandt, Deformation and failure behaviour of Ti-6Al-4V lattice structures manufactured by selective laser melting (SLM), Int. J. Adv. Manuf. Technol. 7 (1) (2015) 20, https://doi.org/10.1007/s00170-015-7655-4.
[12] L. Liu, P. Kamm, F. García-Moreno, J. Banhart, D. Pasini, Elastic and failure response of imperfect three-dimensional metallic lattices: the role of geometric defects induced by Selective Laser Melting, J. Mech. Phys. Solids 107 (2017) 160–184, https://doi.org/10.1016/j.jmps.2017.07.003.
[13] M. Dallago, F. Zanini, S. Carmignato, D. Pasini, M. Benedetti, Effect of the geometrical defectiveness on the mechanical properties of SLM biomedical Ti6Al4V lattices, Procedia Struct. Integrity 13 (2018) 161–167, https://doi.org/10.1016/j.prostr.2018.12.027.
[14] M. McMillan, M. Jurg, M. Leary, M. Brandt, Programmatic lattice generation for additive manufacture, Procedia Technol. 20 (2015) 178–184, https://doi.org/10.1016/j.protcy.2015.07.029.

[15] D. Downing, M. McMillan, M. Brandt, M. Leary, Programmatic lattice generation tools for additive manufacture, Software Impacts 12 (2022) 100262, https://doi.org/10.1016/j.simpa.2022.100262.
[16] D.M. Kochmann, J.B. Hopkins, L. Valdevit, Multiscale modeling and optimization of the mechanics of hierarchical metamaterials, MRS Bull. 44 (10) (2019) 773–781.
[17] O. Al-Ketan, D.-W. Lee, R. Rowshan, A. Al-Rub, K. Rashid, Functionally graded and multi-morphology sheet TPMS lattices: Design, manufacturing, and mechanical properties, J. Mech. Behav. Biomed. Mater. 102 (2020) S. 103520, https://doi.org/10.1016/j.jmbbm.2019.103520.
[18] X. Ma, D.Z. Zhang, M. Zhao, J. Jiang, F. Luo, H. Zhou, Mechanical and energy absorption properties of functionally graded lattice structures based on minimal curved surfaces, Int. J. Adv. Manuf. Technol. 118 (3–4) (2022) 995–1008, https://doi.org/10.1007/s00170-021-07768-y.
[19] D.F. Rogers, J.A. Adams, Mathematical Elements for Computer graphics, second ed., McGraw Hill, New York, 1990. http://www.loc.gov/catdir/description/mh022/89002308.html.
[20] A. Goel, S. Anand, Design of Functionally Graded Lattice Structures using B-splines for Additive Manufacturing, Procedia Manuf. 34 (2019) 655–665, https://doi.org/10.1016/j.promfg.2019.06.193.
[21] L. Paul, J. Favre, B. Piotrowski, S. Kenzari, P. Laheurte, Stress Concentration and Mechanical Strength of Cubic Lattice Architectures, Materials 11 (2018) 1146, https://doi.org/10.3390/ma11071146.
[22] M. Smith, Z. Guan, W.J. Cantwell, Finite element modelling of the compressive response of lattice structures manufactured using the selective laser melting technique, Int. J. Mech. Sci. 67 (2013) 28–41, https://doi.org/10.1016/j.ijmecsci.2012.12.004.
[23] Z.-H. Li, Y.-F. Nie, B. Liu, Z.-Z. Kuai, M. Zhao, F. Liu, Mechanical properties of AlSi10Mg lattice structures fabricated by selective laser melting, Mater. Des. 192 (2020) 108709, https://doi.org/10.1016/j.matdes.2020.108709.
[24] L. Bai, C. Yi, X. Chen, Y. Sun, J. Zhang, Effective Design of the Graded Strut of BCC Lattice Structure for Improving Mechanical Properties, In: Materials 12 (13) (2019) S. 2192, https://doi.org/10.3390/ma12132192.
[25] S. Teufelhart, G. Reinhart, Optimization of strut diameters in lattice structures, in: 23rd Annual International Solid Freeform Fabrication Symposium - An Additive Manufacturing Conference, SFF 2012, 2012, pp. 719–733.
[26] Z. Xiao, Y. Yang, R. Xiao, Y. Bai, C. Song, D.i. Wang, Evaluation of topology-optimized lattice structures manufactured via selective laser melting, Mater. Des. 143 (2018) 27–37, https://doi.org/10.1016/j.matdes.2018.01.023.
[27] E. Träff, O. Sigmund, J.P. Groen, Simple single-scale microstructures based on optimal rank-3 laminates, Struct. Multidisc. Optim. 59 (4) (2019) 1021–1031, https://doi.org/10.1007/s00158-018-2180-3.
[28] D. Taylor, Fatigue-resistant components: What can we learn from nature?, Proc Instit. Mech. Eng. Part C: J. Mech. Eng. Sci. 229 (7) (2015) 1186–1193, https://doi.org/10.1177/0954406214530881.
[29] M. Dallago, V. Fontanari, E. Torresani, M. Leoni, C. Pederzolli, C. Potrich, M. Benedetti, Fatigue and biological properties of Ti-6Al-4V ELI cellular structures with variously arranged cubic cells made by selective laser melting, J. Mech. Behav. Biomed. Mater. 78 (2018) 381–394, https://doi.org/10.1016/j.jmbbm.2017.11.044.
[30] K. Refai, M. Montemurro, C. Brugger, N. Saintier, Determination of the effective elastic properties of titanium lattice structures, Mech. Adv. Mater. Struct. 334 (6058) (2019) 1–14, https://doi.org/10.1080/15376494.2018.1536816.
[31] G. Savio, A. Curtarello, S. Rosso, R. Meneghello, G. Concheri, Homogenization driven design of lightweight structures for additive manufacturing, Int. J. Interact. Des. Manuf 13 (1) (2019) 263–276, https://doi.org/10.1007/s12008-019-00543-0.
[32] Y. Tang, Y. Xiong, S. Park, G.N. Boddeti, D. Rosen, Generation of lattice structures with convolution surface, in: Proceedings of CAD'19. CAD Solutions LLC; 6/24/2019, p. 69–74.
[33] X. Wang, L. Zhu, L. Sun, N. Li, Optimization of graded filleted lattice structures subject to yield and buckling constraints, Mater. Des. 206 (2021) 109746, https://doi.org/10.1016/j.matdes.2021.109746.
[34] R. Ding, B. Du, J. Yao, H. Zheng, Y. Guo, Z. Kang, Mechanical properties and deformation behaviour of ARCH and BCT lattice structures manufactured by selective laser melting, IOP Conf. Ser.: Mater. Sci. Eng. 727 (1) (2020) 012001, https://doi.org/10.1088/1757-899X/727/1/012001.
[35] L. Bai, Y. Xu, X. Chen, L. Xin, J. Zhang, K. Li, Y. Sun, Improved mechanical properties and energy absorption of Ti6Al4V laser powder bed fusion lattice structures using curving lattice struts, Mater. Des. 211 (2021) 110140, https://doi.org/10.1016/j.matdes.2021.110140.
[36] P. Grodzinski, Investigations on shaft fillets, in: Engineering. London, 1941, pp. 321–324.
[37] R.V. Baud, Beiträge zur Kenntnis der Spannungsverteilung in prismatischen und keilförmigen Konstruktionselementen mit Querschnittsübergangen, 1934.
[38] A. Thum, W. Bautz, Der Entlastungsübergang: Günstigste Ausbildung des Überganges an abgesetzten Wellen u. dgl, Forsch Ing-Wes 6 (6) (1935) 269–273, https://doi.org/10.1007/bf02592563.
[39] S. Zelenika, S. Henein, L. Myklebust, Investigation of optimised notch shapes for flexural hinges, in: Proceedings of the 3rd International Workshop on Mechanical Engineering Design of Synchrotron Radiation Equipment and Instrumentation (MEDSI 2004) 2006.
[40] M. Scherrer, Kerbspannung und Kerbformoptimierung: Fakultät für Maschinenbau, Dissertation, Universität Karlsruhe, 2004.
[41] J. Kranz (Ed.), Methodik und Richtlinien für die Konstruktion von laseradditiv gefertigten Leichtbaustrukturen, Springer Berlin Heidelberg, Berlin, Heidelberg, 2017.
[42] C. Mattheck, Teacher tree: The evolution of notch shape optimization from complex to simple, Eng. Fract. Mech. 73 (12) (2006) 1732–1742, https://doi.org/10.1016/j.engfracmech.2006.02.007.
[43] J. Sörensen, Untersuchungen zur Vereinfachung der Kerbformoptimierung, Karlsruhe (2008).
[44] J.T.P. de Castro, D. de Albuquerque Simões, I.F.M. de Menezes, M.A. Meggiolaro, L.F. Martha, A note on notch shape optimization to minimize stress concentration effects, Theor. Appl. Fract. Mech. 84 (2016) 72–85, https://doi.org/10.1016/j.tafmec.2016.03.005.
[45] D. Taylor, A. Kelly, M. Toso, L. Susmel, The variable-radius notch: Two new methods for reducing stress concentration, Eng. Fail. Anal. 18 (3) (2011) 1009–1017, https://doi.org/10.1016/j.engfailanal.2010.12.012.
[46] R.E. Peterson, W.D. Pilkey, Peterson's Stress Concentration Factors, second ed., Wiley, New York, Chichester, 1997.
[47] S. Merkt, R. Poprawe, F. Klocke, Qualifizierung von generativ gefertigten Gitterstrukturen für maßgeschneiderte Bauteilfunktionen: Lehrstuhl für Lasertechnik: Dissertation, RWTH Aachen, 2015.
[48] J. Souza, A. Großmann, C. Mittelstedt, Micromechanical analysis of the effective properties of lattice structures in additive manufacturing, Addit. Manuf. 23 (2018) 53–69, https://doi.org/10.1016/j.addma.2018.07.007.
[49] EOS GmbH: Material data sheet EOS Aluminium AlSi10Mg. https://fathommfg.com/wp-content/uploads/2020/11/EOS_Aluminium_AlSi10Mg_en.pdf. Version: May 2014. – Data sheet
[50] E. Sert, E. Schuch, A. Öchsner, L. Hitzler, E. Werner, M. Merkel, Tensile strength performance with determination of the Poisson's ratio of additively manufactured AlSi10Mg samples, Materialwiss. Werkstofftech. 50 (5) (2019) 539–545, https://doi.org/10.1002/mawe.201800233.
[51] DIN 3369, Impermeable sintered metal materials and hard metals - Determination of density (DIN 3369:2010), German Institute for Standardization, 2010.
[52] DIN 50134, Testing of metallic materials - Compression test of metallic cellular materials (DIN 50134:2008-10), German Institute for Standardization, 2008.
[53] J. Weidmann, A. Großmann, C. Mittelstedt, Laser powder bed fusion manufacturing of aluminum honeycomb structures: Theory and testing, Int. J. Mech. Sci. 180 (2020) 105639, https://doi.org/10.1016/j.ijmecsci.2020.105639.
[54] M. Dallago, S. Raghavendra, V. Luchin, G. Zappini, D. Pasini, M. Benedetti, The role of node fillet, unit-cell size and strut orientation on the fatigue strength of Ti-6Al-4V lattice materials additively manufactured via laser powder bed fusion, Int. J. Fatigue 142 (2021) 105946, https://doi.org/10.1016/j.ijfatigue.2020.105946.
[55] Association of German Engineers, VDI 3405 Part 3, Additive manufacturing processes, rapid manufacturing Design rules for part production using electron beam melting, Beuth Verlag, Berlin, 2015.